THE BEAM DELIVERY SYSTEM OF THE EUROPEAN SPALLATION SOURCE*

H.D. Thomsen†, S.P. Møller, Dept. of Physics and Astronomy, Aarhus University, Aarhus, Denmark

Abstract

The European Spallation Source (ESS) will apply a fast beam scanning system to redistribute the proton beam transversely across the spallation target surface. The system operates at sweep frequencies of tens of kHz and efficiently evens out the time-averaged beam intensity within a nominal beam footprint, thus reducing the level of beam-induced material damage. A modular design approach divides the raster action in each direction across 4 independent magnet-supply systems to distribute the magnetic load, ease the peak output power per modulator, and in general reduce the impact of single point of failures (SPOFs). The state of the magnet design and power supply topology will be discussed.

INTRODUCTION

Several present and future accelerator projects at the intensity frontier feature an accelerator (linac or cyclotron) that delivers a MW-class beam to a fixed target for *e.g.* secondary beam production or reactors. Common to all such projects is the importance of the accelerator–target interface, where many challenges and compromises are to be dealt with, and the Accelerator-to-Target (A2T) section of the ESS is no exception. To be able to sustain the considerable beam power, the beam is here expanded to a substantial size to minimize the local power deposition and radiation-induced material degradation across the target shroud and accelerator vacuum windows, if relevant. The replacement frequency of such components and the capacity of their associated cooling systems can be reduced even more by applying schemes to produce transverse beam current profiles that are close to uniform with an extent that matches the edges of beam confinement regions, beyond which only fractions of beam are tolerated. These sophisticated Beam Delivery Systems (BDSs) include both a linear expansion (relying on magnetic quadrupoles) and a system to intentionally distort the time-averaged beam profiles by applying *e.g.* non-linear or AC dithering fields. Several facilities have considered such systems, as will be discussed. Given the considerable beam currents often involved, excessive uncontrolled primary beam losses may ensue, if these systems are not properly designed or the incoming beam is significantly different from the assumptions made in the design phase.

Non-Linear Magnets

To flatten high-power ion beams using a system of non-linear magnetic lenses has long been studied [1], [2], [3], [4], [5], [6] and even applied at *e.g.* the NASA Space Radiation Laboratory, BNL [7], [8]. The scheme will be applied to existing (J-PARC [9]) and future facilities (CSNS, C-ADS, IFMIF [10]). The systems include either pure multipole elements ($O(2n)$ pole elements with $n \geq 3$, *i.e.* sextupoles, octupoles, *etc.*.) or rely on more specialized combined function magnets, *e.g.* the so-called dipole pairs [1] or step-like field magnets [4] which are based on relatively similar magnet topologies. Considering *e.g.* a horizontally Gaussian beam profile with an elliptical phase space distribution (x, x') , a properly applied octupole magnetic field ($B_y(x, y) \propto x^3$) will introduce a symmetric horizontal focusing force affecting in particular the beam tails, causing a characteristic S-shape in the phase space. Although the solution can provide close to uniform distributions by applying DC fields, there are several caveats.

Overfocusing: Unless compensated, the strong non-linear forces can severely overfocus halo particles, which may lead to excessive losses before the beam reaches its intended destination. Saturating the field strengths at large excursions, either by combined-function magnet design or introducing *e.g.* dodecapoles, can compensate for this [1].

Lack of flexibility: Non-linear magnets are usually designed with a narrow band of not only beam RMS sizes in mind, but also kurtosises, *i.e.* beam quality, something that can be very difficult to predict before the accelerator is constructed and commissioned. Combined-function magnets offering several degrees of freedom [11] can perhaps efficiently cover a span of kurtosises.

Beam-magnet alignment: In particular the pure non-linear magnets are very sensitive to beam-magnet displacement, giving rise to steering errors and beam profile artefacts, *e.g.* the characteristic "ears" near the profile edges, in case of octupoles [1].

Aperture vs. field: Designing the non-linear magnets also involves the trade-off between having a sufficient impact on the beam, while retaining sufficiently large apertures to avoid beam losses. This balance becomes increasingly difficult with an intense, rigid beam.

Coupling: To enable flattening of both the horizontal (H) and vertical (V) profile, dedicated H and V non-linear lenses should be applied at locations where the beam RMS size aspect ratio is large, ($\sigma_x/\sigma_y \gg 1$ in the H multipole and vice versa) to avoid H–V coupling. The scheme thus requires magnetic elements between the two non-linear elements. Depending on the beam emittance and tuning accuracy, the beam waists cannot provide complete H-V decoupling, thus rendering tuning complicated.

* Work supported by European Spallation Source ERIC
† heinetho@phys.au.dk

ISBN 978-3-95450-178-6

To assess the concept of applying a multipole-based BDS for a high-power accelerator, the Los Alamos National Lab (LANL) Accelerator Production of Tritium (APT) project, two prototype magnets were constructed for testing at the 800 MeV LANSCE/LAMPF [11]. Both magnet prototypes were 500 mm long 12-pole magnets with three independent families of coils to vary the octupole and dodecapole components while cancelling the quadrupole component. A large beam aspect ratio (3 mm / 25 mm) was assumed when designing the non-cylindrical aperture. Using Hall probes at LANL and a rotating coil system at BNL, the measured field profiles were found to match the calculated values quite well [11]. Even so, "prompt beam-loss radiation was detected near the two nonlinear octupoles" when testing with a pulsed proton beam of 0.1 µA average current or 80 W average power [12]. The observed loss rates would be intolerable, if scaled to APT's 170 MW average beam power. Even before the prototype testing, it was decided to use a linear raster system for the APT instead. This may have had an impact on the beam time allotted for the multipole testing where more extensive commissioning of the system could perhaps have improved the loss levels. The main drivers were the more straightforward tuning of the system and reduction of the expected beam losses.

Much like the LANL story, a great effort was put into studying a multipole-based BDS for the ESS [13], in particular balancing the obtained flattening of beam profiles and the induced losses. To compensate for the latter, a collimator close to the target was intended to intercept of the order of tens of kW of primary beam, even when assuming a nominal beam from the accelerator. The ESS multipole studies confirmed that tuning the non-linear elements was extraordinarily sensitive to the input beam distribution, specifically the magnitude and extent of the beam's tails, or halo. To optimize the settings would involve a series of time-consuming particle tracking simulations. The concept's sensitivity towards beam quality can be considered as a considerable risk, when designing a new facility, in particular when aiming for unprecedented machine parameters or application of novel acceleration technologies, whereas it may be more straightforward to retrofit them into an existing beam line [9]. Due to the reasons above, the ESS BDS was changed to be raster-based in mid-2013.

Raster Systems

As an alternative to non-linear magnets, a set of AC dipole raster magnets can be applied to introduce suitable H and V displacement waveforms at a downstream location, *e.g.* a target surface, such that the beam centroid is swept in a two-dimensional (2D) displacement pattern. A true raster pattern would necessitate a rapid scan in one direction, while the orthogonal scan would be a slower series of steps that match the rapid scan period. This scheme thus demands two distinct magnet and power supply designs. Instead, a common design can typically be used, if the H and V raster waveforms have either identical frequencies but are dephased (thus generating a circle or ellipse) or frequencies corresponding to coprime harmonics, thus generating a Lissajous-like pattern, with a ratio close to but different from unity. Independent linear DC beam optics (*i.e.* quadrupoles) sets the size of the beamlet that is scanned in a controlled pattern, and the resulting time-averaged beam intensity distribution would be a convolution of the displacement pattern and the beamlet profile. The uniformity of the resulting distribution will depend on the spacing between the respective sweeps relative to the beamlet size. The raster waveform amplitude thus sets the size of the central uniform area, while the beamlet RMS size determines the shape and extent of the distribution edges. A pattern containing several sweeps in both directions of a suitably sized beamlet can thus produce effective distributions that inherently suppresses the impact of variations in the incoming beam's profiles. This attractive BDS feature is quite contrary to a system based on multipoles.

Table 1: Nominal Beam Parameters and Requirements at the ESS Target Surface [20]

Parameter	Unit	Value
Average beam power	MW	5.0
Final kinetic energy	GeV	2.0
Beam rigidity	T.m	9.29
Peak beam current	mA	62.5
Average beam current	mA	2.5
Pulse repetition rate	Hz	14
Duty cycle	%	4
Pulse duration	ms	2.86
Maximum beam offset $\langle x \rangle$	mm	±5
Maximum beam offset $\langle y \rangle$	mm	±3
Nominal $\langle J(x,y) \rangle$	µA/cm^2	56
Maximum $\langle J(x,y) \rangle$	µA/cm^2	71
99.0% H × V footprint	mm^2	160 × 60
99.9% H × V footprint	mm^2	180 × 64
Min. $\sigma_x \times \sigma_y$	mm^2	50
Min. hor. raster frequency	kHz	35

Since the scanning pattern will have an inherent finite cycle period, raster systems are most appropriate for accelerators providing long-pulsed or CW beam, and both MYRRHA [14] and SINQ [15] are designing circular raster systems operating at tens to hundreds of Hz to reduce the peak current density on the beam windows and targets. Apart from being designed to be a CW machine, there is a great resemblance between the beam parameters of the APT and the ESS. The raster system designed and prototyped for the APT has thus served as a great inspiration. Whereas the APT system was designed to operate in the 500 Hz–600 Hz range [16], [17], [18], the ESS system will operate at considerably larger frequencies, 10 kHz–40 kHz [19], [20].

The ESS Beam on Target Requirements

The nominal and required beam parameters at the rim of the ESS target wheel rotating at 0.4 Hz [20] can be inspected in Table 1. The listed parameters, *e.g.* the beam

ISBN 978-3-95450-178-6

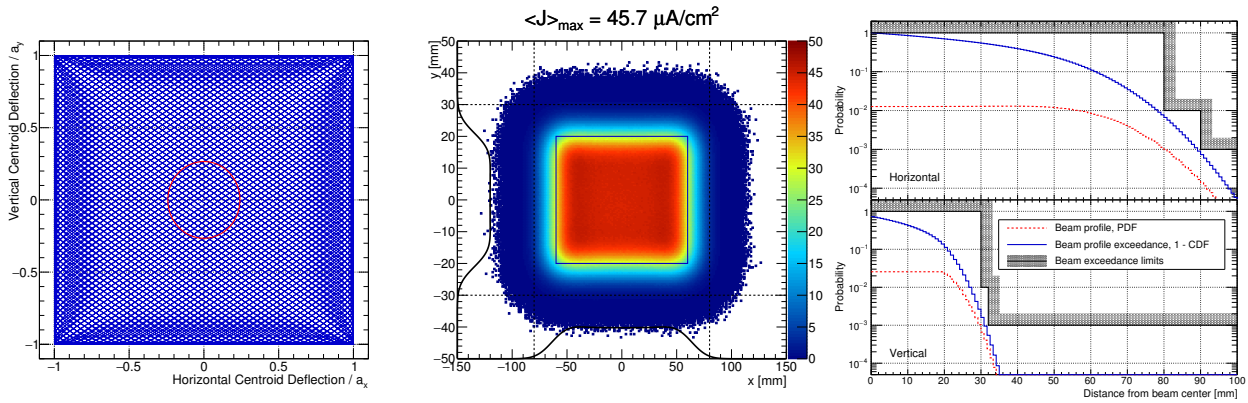

Figure 1: Left panel: A $f_x/f_y = 113/83$ raster pattern compared to the 1-RMS beam size ellipse. Middle panel: A simulation of $\langle J(x,y)\rangle$ with the projected profiles (black curves) and raster pattern outline (blue box). $(a_x, a_y, \sigma_x, \sigma_y) = (60, 20, 12, 4.5)$ mm. The dashed lines mark the 99% confinement zone. Right panel: Diagrams showing the horizontal and vertical PDF and CCDF = 1 − CDF compared to the confinement requirements of Table 1.

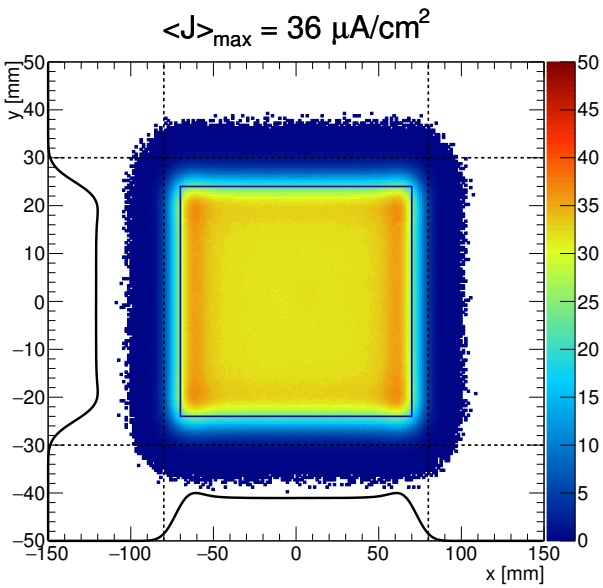

Figure 2: $(a_x, a_y, \sigma_x, \sigma_y) = (70, 24, 7, 3)$ mm.

profile offset from nominal center, $\langle x\rangle$ and $\langle y\rangle$, relate to the pulse-averaged delivered beam, *i.e.* covering a full nominal $(14\,\mathrm{Hz})^{-1}$ beam pulse cycle. The time-averaging does not take the rotation of the target into account. The average current density $\langle J(x,y)\rangle = \int J(x,y,t)\mathrm{d}t$ is a representation of a two-dimensional PDF scaled with the average beam current. It should be emphasized that there are no requirements regarding the distribution's flat top uniformity per se, but that the combination of limiting $\langle J(x,y)\rangle$ while setting confining footprints, truly entails a method to make the profiles very close to uniform.

Optimizing Parameters

With a raster-based system, the degrees of freedom in tailoring the resulting distribution are the raster frequencies (f_x, f_y), the displacement amplitudes (a_x, a_y), and the DC beamlet beam RMS size (σ_x, σ_y). If the sweep frequencies are chosen such that the raster pattern is finely meshed with a centroid path spacing less than (σ_x, σ_y), the time-averaged pulse will not contain artefacts, *i.e.* intensity modulations, due to the raster pattern. For such raster distributions, the amplitudes determine the full width at half maximum (FWHM) of the distribution, *i.e.* the general edge of the distribution. The sharpness of the edge around this point, and the extent of the distribution's tails relative to the amplitudes, will be characterized by the choice of (σ_x, σ_y). To keep the beam confined while providing sufficient rastering is thus a matter of optimizing *e.g.* (a_x, σ_x) where the parameters should be treated as inversely correlated. As an additional constraint, a considerable minimum beamlet cross section $\sigma_x \times \sigma_y > 50\,\mathrm{mm}^2$ is required to ensure that the shroud of the rotating target is unlikely to rupture in the event of a complete failure of the raster system.

Raster patterns have been generated by sampling 2^{16} points from triangle waveforms over a 2.86 ms duration. The pure waveforms are passed through a 1st order Butterworth filter with an upper cutoff frequency $f_{c,2} = 200$ kHz. Assuming prime harmonics of the fundamental pulse frequency, $f_x = 113/2.86\,\mathrm{ms} = 39.6\,\mathrm{kHz}$ and $f_y = 83/2.86\,\mathrm{ms} = 29.1\,\mathrm{kHz}$, the coordinates of the raster pattern is used for Monte Carlo simulations of the resulting beam distribution. At each centroid coordinate, 10^4 protons are sampled from a 2D Gaussian with (σ_x, σ_y) and the data is projected onto a 2D histogram and scaled to represent $\langle J(x,y)\rangle$. This quantity is minimized by searching in the two decoupled parameter spaces (a_x, σ_x) and (a_y, σ_y). It is important to stress that a_x and σ_x are controlled independently in the real accelerator, by the raster system and DC quadrupoles, respectively. An example of the Monte Carlo simulations is represented in Fig. 1. To evaluate the confinement of the simulated protons, the distribution profiles (*i.e.* PDFs), and the resulting exceedance (tail distribution, or complementary cumulative density function (CCDF)) are evaluated and compared to the 99% and 99.9% limits, cf. right

ISBN 978-3-95450-178-6

panel of Fig. 1. In both H and V, the exceedance of the beam profiles is seen to closely match these limits. In the example, $(a_x, a_y, \sigma_x, \sigma_y) = (60, 20, 12, 4.5)$ mm, *i.e.* $\sigma_x \times \sigma_y = 54\,\mathrm{mm}^2$. The local intensity could further be reduced if smaller beamlet cross sections would be tolerated. As the beamlet sizes are lowered, however, the profiles begin to exhibit distinctive intensity ridges ridges that are characteristic of the finite bandwidth of the raster waveforms, cf. Fig. 2, which causes the beam to linger near the edges. The horizontal waveform is particularly affected since $f_x/f_{c,2} > f_y/f_{c,2}$. Although there is a benefit in $\langle J(x,y)\rangle$ from the smaller beamlet cross section, there is thus a limited benefit in seeking lower numbers, which in addition would severely increase the impact of a full failure of raster system. It should be emphasized that it has not been studied whether the DC beam optics of the ESS A2T is able to provide *e.g.* $(\sigma_x, \sigma_y) = (7, 3)$ mm at the target surface.

SYSTEM DESCRIPTION

At the required raster frequencies of >35 kHz in the horizontal direction [20], full magnetic field waveform control becomes unfeasible. Instead, it is exploited that when applying a voltage waveform across a purely inductive load, the resulting current waveform passing through the load will be of a temporal shape that is equivalent to the integral of the voltage waveform. The required symmetric triangle current waveform can thus be generated by applying a square voltage waveform across the load. The load in this context, *i.e.* the raster magnets and the cables carrying the AC currents, can be designed to resemble a predominantly inductive load, while still maintaining a low enough inductance to permit AC currents at tens of kHz.

A modular design approach is followed by distributing the required raster action over a string of colinear Raster Scanning Magnets (RSMs) placed in pairs of identical field direction, $(B_yB_y)(B_xB_x)(B_xB_x)(B_yB_y)$, *i.e.* a set of four acting in H, four acting in V, with a central point of symmetry. Each of the RSMs in a set are to be synchronized within ±200 ns and divide the field amplitude evenly. Although this would enable powering the RSMs in a set with a single supply, each RSM is powered by a dedicated modulator. The individual powering reduces the magnetic load on the RSMs and the peak output power of each modulator, but it is also a straightforward approach to reduce the impact of element failures by implementing redundancy. By operating the system at a duty cycle of only 5%, appropriately more than the 4% beam pulse duty cycle, active cooling of magnets and modulators is unnecessary, thus providing a higher reliability.

Magnet Design

A cross section and isometric view of a H RSM (*i.e.* with a vertical field component) can be seen in Fig. 3. The magnet design features a NiZn ferrite-based yoke to accommodate the considerable operating frequency. Several commercially available ferrites, *e.g.* CMD5005 from National Magnetics

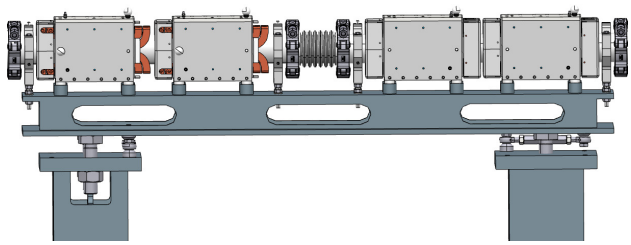

Figure 3: Sagittal cross section of a RSM with dimensions in mm (left, top panel) and isometric view of a complete RSM (right, top panel). Ferrite parts are shown in turquoise and are held in place by spring-loading them against a metallic housing. The bottom panel shows a 4-magnet setup based on a girder that rests on a pair of supports.

Table 2: Top Level Parameters and Specifications of a RSM

Parameter	Unit	Value
Min. magnet aperture	mm	100
Magnetic length	mm	300
Turns per coil	—	2
Peak strength	mT.m	5
Nom. strength $B\ell$ (H / V)	mT.m	1.5 / 2.6
Nom. deflection (H / V)	mrad	0.16 / 0.28
Max. current (peak-to-peak)	A	±340
Max. voltage (peak-to-peak)	V	±650

Group (formerly Ceramic Magnetics), offer sufficiently low eddy current losses and a high frequency response. The Cu coils are cut from a 1 mm thick OFHC plate and bent into 2-turn bedstead coils. The plate thickness is chosen as a trade-off between minimizing eddy current power losses, the Cu skin depth is $\delta_x = 0.3\ \mathrm{mm} \times \sqrt{40\ \mathrm{kHz}/f_x}$, while maintaining structural integrity considering being subjected to the AC magnetic forces. A window-frame magnet yoke design is chosen to provide very uniform fields across almost the entire magnet aperture, thus minimizing the pole width and avoiding the pole shims involved in an H-magnet. This topology not only minimizes the magnet production cost but also reduces the power supply specifications. One potential disadvantage of the considerable extent of the magnetic fields inside the magnet aperture is that the AC fields would induce eddy current in the actual coils, which in turn could result in power losses and field strength and quality degradation. This effect has not yet been studied but pushes for as thin coils as mechanically possible. The magnet parameters can be found in Table 2. The magnet gap of 100 mm is chosen to avoid significant physical aperture restriction in the

ISBN 978-3-95450-178-6

ceramic vacuum chambers along the RSMs. Having set this figure, the physical length should be chosen appropriately larger to reduce the impact of the inevitable fringe field's inferior field quality. Additionally, the system's stored energy (and thus the concomitant supply's VA rating) will be inversely proportional to the magnet length. The current design features a 230 mm magnet yoke, the longest possible to avoid spatial conflicts.

To facilitate installation, alignment/realignment, and the replacement of principal elements, a girder-based support stand is proposed. There will be two stands holding 4 RSMs each, cf. bottom panel of Fig. 3. High-precision RSM position slots are expected to be machined along the girder, thus avoiding the need for individual RSM alignment, while the girder is used to align the 4 RSMs simultaneously. In case of having to replace a RSM or a vacuum chamber, the vacuum system can be disconnected using quick-CF flanges, and the entire girder can be hoisted out for maintenance, thus minimizing maintenance crew's occupation and exposure to activated components in the accelerator tunnel.

While raster magnets can be produced to sustain the radiation levels that are expected in the tunnel, the power supplies will contain electronics with radiation resistance that are not suitable for radiation zones. The power supplies will thus need to be located at an appropriate distance from the tunnel. The power cables connecting each magnet and supply are foreseen to be 30 m long.

Power Supply Design

Each RSM is powered by a dedicated supply, or modulator, based on a capacitor-charging supply (input converter) and an H-bridge (output converter) to generate the required square voltage waveform across the RSM. More details can be found in [21]. The four semiconductor power switches constituting the H-bridge could be either IGBTs or MOSFETs. Besides, each supply will contain local control electronics (a microprocessor for internal control and communication with the Integrated Control System (ICS)) and a feedback/regulation controller. The latter will be a FPGA to regulate the signals for the switch drivers and the waveform amplitudes, *i.e.* the capacitor voltage. The rise time of the H-bridge switches, t_r, is believed to be the major contributor to $f_{c,2}$, being of the order of $t_r \simeq 250$ ns. A previous study found that the minimum value of $f_{c,2}$ should be the fifth harmonic, or 200 kHz [21].

Fault Detection & Mitigation

In particular when consisting of dynamic elements, closely monitoring the performance of the BDS is imperative to prevent component damages and support the 95% availability requirement of the ESS. Potential malfunctions should be foreseen and mitigated internally, if possible. Simple preventive measures like monitoring internal component temperatures, the capacitor voltage, controller state, *etc.* will be an integral part of the local protection functions implemented in each supply. A pretrigger initiates a RSM supply preparatory phase that precedes each raster pulse. The phase duration should allow for extensive system verification that produces an active "ready for beam?" signal to the ESS Run Permit System (RPS). Detection of a local state that could give rise to a non-nominal beam condition shall provoke an interlock signal for the ESS Beam Interlock System (BIS), which can inhibit further beam production and transport at low energies. Apart from the internal local protection functions implemented in each supply, a dedicated ESS RSM Fault Detection Unit (FDU) is to monitor the performance of the RSMs and interfaces to the RPS and BIS. Each RSM will feature a Bdot loop, which typically consists of a single wire back-leg or pole-face winding. A current that is proportional to the rate of change in magnetic flux through the loop will be induced. The resulting voltage square waveforms are a direct consequence of the magnetic fields and thus constitute a valuable indicator of the system's performance in terms of perturbing the beam. Additionally, each supply could contain Idot loops (a current transformer) that measures the rate of change in cable current, *i.e.* ideally also a square waveform. Such signals are obvious input candidates for the RSM FDU, as has been done in other raster magnet applications [22].

Even if a failure should remain undetected, the detailed design study is attempting to push the 4-fold redundancy to as high a level as reasonable and purge the system of single point of failures (SPOFs). In case of a sudden and complete failure in one RSM subsystem, 75% amplitude should be maintained in the affected direction, giving rise to a 33% increase in $\langle J(x, y)\rangle$, which is tolerable for longer durations, cf. Table 1. Even in the catastrophic event of a complete failure of the entire RSM system, letting an unrastered beamlet on the target, the sheer target rotation will allow for mitigation times as long as $\simeq 2$ s [20], assuming $\sigma_x \times \sigma_y > 50\,\mathrm{mm}^2$.

To support the 95% availability requirement, a considerable field strength amplitude contingency of almost 100% in each subsystem, cf. Table 2, enables continued operation in a degraded mode having even a few of the RSM subsystems offline.

OUTLOOK & CONCLUSION

A raster-based BDS is being designed to provide a beam that conforms to the ESS beam-on-target requirements. Although studies of the application of DC multipoles have been made previously, the raster-based system is found to be superior in several aspects. This should, however, be expected to depend considerably on the parameters and requirements of the facility in question. As of June 1st, 2016, a contract has been signed with the vendor that also carried out a feasibility study of the system, Danfysik. Although the parameters appear practical from simulations, a complete two-magnet pre-series will be constructed and tested ultimo 2017. The full series should finish production by the end of 2018 and be installed at ESS in March, 2019.

ISBN 978-3-95450-178-6

REFERENCES

[1] B. Blind, "Production of uniform and well-confined beams by nonlinear optics," *Nucl. Inst. and Meth. in Phys. Research B*, vol. 56-57, Part 2, pp. 1099–1102, 1991.

[2] E. Urakabe, Y. Fujita, K. Hiramoto, *et al.*, "Beam-profile control using an octupole magnet," *Japanese Journal of Applied Physics*, vol. 38, pp. 6145–6149, 1999.

[3] F. Meot and T. Aniel, "Principles of the non-linear tuning of beam expanders," *Nucl. Inst. and Meth. in Phys. Research A*, vol. 379, no. 2, pp. 196–205, 1996.

[4] J. Tang, H. Li, S. An, and R. Maier, "Distribution transformation by using step-like nonlinear magnets," *Nucl. Inst. and Meth. in Phys. Research A*, vol. 532, no. 3, pp. 538–547, 2004.

[5] J. Tang, G. Wei, and C. Zhang, "Step-like field magnets to transform beam distribution at the CSNS target," *Nucl. Inst. and Meth. in Phys. Research A*, vol. 582, no. 2, pp. 326–335, 2007.

[6] Y. Yuri, N. Miyawaki, T. Kamiya, W. Yokota, K. Arakawa, and M. Fukuda, "Uniformization of the transverse beam profile by means of nonlinear focusing method," *Phys. Rev. ST Accel. Beams*, vol. 10, p. 104 001, Oct. 2007.

[7] N. Tsoupas, L. Ahrens, S. Bellavia, *et al.*, "Uniform beam distributions at the target of the NASA Space Radiation Laboratory's beam line," *Phys. Rev. ST Accel. Beams*, vol. 10, p. 024 701, 2 Feb. 2007.

[8] N. Tsoupas, S. Bellavia, R. Bonati, *et al.*, "Results from the Commissioning of the NSRL Beam Transfer Line at BNL," in *Proc. EPAC 2004, Lucerne, Switzerland*, 2004, pp. 2879–2881.

[9] S. Meigo, A. Akutsu, K. Ikezaki, M. Ooi, and H. Fujimori, "Beam Flattening System based on Non-linear Optics for High Power Spallation Neutron Target at J-PARC," in *Proc. IPAC'14*, 2014, p. 896.

[10] Z. Yang, J. Tang, P. P. Nghiem, and N. Chauvin, "Using Step-Like Nonlinear Magnets for Beam Uniformization at IFMIF Target," in *Proceedings of HB2012, Beijing, China*, 2012, p. 424.

[11] D. Barlow, R. Shafer, R. Martinez, *et al.*, "Magnetic design and measurement of nonlinear multipole magnets for the APT beam expander system," in *Proc. PAC'97*, May 1997, pp. 3309–3311.

[12] R. E. Shafer, "Comment on "uniformization of the transverse beam profile by means of nonlinear focusing method"," *Phys. Rev. ST Accel. Beams*, vol. 11, p. 039 001, 3 Mar. 2008.

[13] A. Holm, H. D. Thomsen, and S. P. Møller, "The Layout of the High Energy Beam Transport for the European Spallation Source," in *Proc. IPAC'12 New Orleans, USA*, 2012, p. 475.

[14] H. Saugnac, J. Biarrotte, L. Perrot, D. Vandeplassche, and A. Ferrari, "High Energy Beam Line Design of the 600 MeV, 4 mA proton Linac for the MYRRHA Facility," in *Proc. IPAC'11*, 2011, p. 2721.

[15] T. Reiss, D. Reggiani, M. Seidel, V. Talanov, and M. Wohlmuther, "Simulation of a beam rotation system for a spallation source," *Phys. Rev. ST Accel. Beams*, vol. 18, p. 044 701, 4 Apr. 2015.

[16] C. R. Rose and R. E. Shafer, "A 200-A, 500-Hz, triangle current-wave modulator and magnet used for particle beam rastering," in *Proc. PAC'97*, 1997, pp. 1293–1295.

[17] S. Chapelle, E. L. Hubbard, S. T. L., M. E. Schulze, and R. E. Shafer, "Development of a Raster Electronics System for Expanding the APT Proton Beam," in *LINAC'98*, May 1998, p. 612.

[18] S. Chapelle, S. T. L., D. J. LeBon, M. E. Schulze, and R. E. Shafer, "Testing of a Raster Magnet System for Expanding the APT Proton Beam," in *Proc. of PAC'99*, 1999, p. 3758.

[19] T. Shea, K. Andersen, P. Bentley, *et al.*, "Design Considerations for the ESS Accelerator-to-Target Region," in *Particle Accelerator Conference, 2013*, 2013, p. 300.

[20] E. Pitcher and T. Shea, "Beam on target requirements," European Spallation Source, Tech. Rep. ESS-0003310, 2015.

[21] H. Thomsen and S. Møller, "The Design of the Fast Raster System for the European Spallation Source," in *Proc. IPAC'14*, 2014, p. 2118.

[22] R. Sheffield and M. E. Schulze, "Raster Magnet System for Expanding the APT Proton Beam," Los Alamos National Laboratory, Tech. Rep. LA-UR-99-5820, 1999.

ISBN 978-3-95450-178-6